Check for updates

Incoherent scattering from dielectric metasurfaces under the influence of electromagnetic eigenmodes

R. S. Puzko,[1,2] **D. N. Kozlov,**[1,3] **V. I. Fabelinsky,**[3] **Y. N. Polivanov,**[3] **V. V. Smirnov,**[3] **A. K. Sarychev,**[4] **I. A. Ryzhikov,**[4,5] **H. V. Bandarenka,**[6] **and A. M. Merzlikin**[2,4,*]

[1]*Moscow Institute of Physics and Technology, 9 Institutskiy per., Dolgoprudny, Moscow Region 141700, Russia*
[2]*All-Russia Research Institute of Automatics, Sushchevskaya st., 22, Moscow 127055, Russia*
[3]*Prokhorov General Physics Institute of the Russian Academy of Sciences, Vavilov st. 38, Moscow 119991, Russia*
[4]*Institute for Theoretical and Applied Electromagnetics, Russian Academy of Sciences, Izhorskaya st., 13, Moscow 125412, Russia*
[5]*Bauman Moscow State Technical University, 2nd Baumanskaya st., 5/1, Moscow 105005, Russia*
[6]*Laboratory of Materials and Structures of Nanoelectronics, Belarusian State University of Informatics and Radioelectronics, 6 Brovka St., Minsk 220013, Belarus*
*merzlikin_a@mail.ru

Abstract: Anomalous optical properties of microscopically inhomogeneous dielectric films placed on a thick metal sublayer are investigated. We study the reflection, scattering, and absorption of the coherent electromagnetic radiation as a function of the incidence angle. Computer simulations show the existence of the incidence angle of the laser beam when the scattering and absorption increase simultaneously for the s-polarization so that almost 60% of the incident light goes in the scattering channel. The critical angle corresponds to the excitation of Fabry-Perot mode. The effect makes it possible to manipulate the reflection from the metafilms.

1. Introduction

The light scattering by inhomogeneities presents interest for various fields of physics and engineering, ranging from astronomical and atmospheric studies [1,2] to applications in medicine and technology (increase in solar cell efficiency [3], analyses of biological samples [4], etc.). Two important cases of light scattering are discussed in the literature: volume scattering in an inhomogeneous medium [5–7] and scattering by the sample boundaries' roughness [8–11].

In the case of volume scattering (a transparent host with some inclusions), the electromagnetic wave propagation through the medium containing volume inhomogeneities is considered [12–17]. Particular attention is paid to the light scattering inside the bounded structures where it is possible to identify regions with different optical properties. For example, the light scattering in the multilayer structures is considered in [13,18–20].

The light scattering from a rough surface was studied in detail by many authors [9–11,21–32]. Surfaces with small height fluctuations (in comparison with the illumination wavelength) are considered in theoretical works as a rule. Small fluctuations allow one to construct perturbation theory [11,27] or an equivalent method of the stochastic functional [21,22]. These approaches were used in [11,22] to study single and double scattering processes in detail (in particular, the effects of backward coherent scattering and satellite peaks). Particularly it was shown the increasing of scattering near the angle of total external reflection (the so-called Yoneda peaks) [29–32] and the influence of field distribution on this scattering

was also discussed [29]. The anomalous light scattering from metal-dielectric metafilms was considered in [33,34] for the case of the collective plasmon resonance.

It is worth noting here that two problems can be distinguished: light scattering by the roughness of a half-space boundary [28,30,32] and light scattering by rough boundaries of structured samples, in particular, layered systems [22,25,27]. In the latter case, the light scattering is significantly affected by the system modes. For example, the effect of resonant scattering was discovered in the layered system supporting the guided modes [8]. The resonant scattering occurs at certain angles of guided mode excitation. Experimental investigations of scattering spectra for films with rough surfaces are presented in [8,35].

The presence of the system eigenmodes results in unusual scattering features. Electromagnetic resonances can be excited in any piece of a low loss dielectric. Yet, the Q factor is quite different for various modes. It should be noted that a high contrast of the material dielectric permittivity and the small Ohmic losses can result in dielectric resonances with a high Q-factor.

This paper is devoted to a theoretical investigation of laser light scattering inside CeO_2 films. The films might be produced by electron-beam deposition in vacuum [36]. It is worth noting that a CeO_2 films structure possesses complex morphology, in particular a faceted one [36]. A complex nanostructure of a CeO_2 films can significantly affect optical properties [37,38]. Furthermore, light scattering by film inhomogeneities can lead to an effective attenuation of coherent radiation. In the present paper we propose a simple model of light scattering by inhomogeneities. The model reproduces interesting features of the scattering and reflection of the considered surface coating. This research was initiated by experimental studies which will be presented elsewhere.

The paper is organized as follows. Firstly, we described the investigated dielectric metasurface. Then, a theoretical model for the light scattering is proposed. The theoretical consideration starts with the case of weak scattering, when the intensity of the light scattered by inhomogeneities is negligibly small in comparison with that of the incident light. Then the scattering parameter used in calculations is introduced and the strong scattering is studied. Finally, the angular dependences of scattering amplitudes are discussed in connection with the eigenmodes of the system. The results are briefly summarized in conclusion.

2. Coating structure

The considered system is displayed in Fig. 1. The inhomogeneous dielectric film is placed onto a metal layer. The laser beam illuminates the sample at different angles. The density inhomogeneity of the coating acts as a scatterer for the incident light. Cerium dioxide is the material of the scattering layer. The randomness in inhomogeneities positions as well as randomness in their shapes result in the spatially incoherent scattering. Cerium dioxide is the material of the scattering layer. The choice of the material is made for two reasons. Firstly, cerium dioxide being a transparent material has a high value of refractive index. The high refractive index leads to the stronger scattering as the contrast between the air and dielectric becomes more evident. Secondly, the films manufactured of cerium dioxide possess complicated microstructure [37–43]. The metal layer is made of aluminum.

Film microstructure strongly depends on manufacturing technology. Unfortunately, the produced films contain some amount of inhomogeneities, leading to the light scattering and the degradation of multilayer coating properties. However, that deficiency of technology might be turned to the advantage in some applications. In particular, the structure in Fig. 1 used as scattering coating, can significantly change the reflection properties (as it will be shown below).
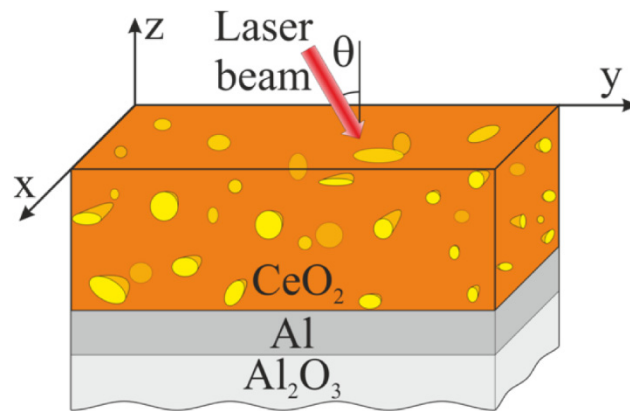
Fig. 1. Schematic representation of the considered coating.

3. Light scattering by volume inhomogeneities

We consider the scattering in a dipole approximation: the incoherent radiation emitted by an inclusion or inhomogeneity in the dielectric film is treated as the emission of a dipole induced by a coherent external field. Due to the coherent radiation scattering, a part of the coherent beam energy transforms into spatially incoherent scattered radiation energy. Therefore, the coherent part of the radiation decreases as the beam propagates through the material. The radiation scattered by different dipoles will be considered incoherent. This important simplification takes into account only single scattering processes and neglects multiple scattering ones. This approximation is valid for the propagation length of radiation inside the system smaller than its mean free path. In the calculations, we assume that the dipoles representing inhomogeneities (the volume fluctuations of the refractive index) are uniformly distributed within the film volume.

First we consider a **model system** in which the scattering is weak and the light attenuation on the layer thickness is insignificant. This assumption is justified if the scattering cross section of inhomogeneities and their concentration are so small that the scattered energy is significantly smaller than the Ohmic losses in the systems. Then we proceed to the case of strong scattering to evaluate the influence of scattering on the reflection coefficient.

3.1. Weak scattering case

In this section, we assume that the scattering is weak and the energy of the incident coherent radiation does not decrease due to scattering, that is, all the dipoles are in the field of such an external wave as they would be in the absence of scattering.

In the long-wavelength approximation, a dipole moment of a single scatter is directly proportional to the local electric field. To calculate the scattered field in the given geometry, it is convenient to proceed to the plane wave basis by expanding the dipole radiation into plane waves with different propagation directions and polarizations. Then, the electromagnetic field induced by a dipole in the system (and the scattered radiation field) can be found by considering the propagation through the system of each plane wave, generated by the dipole. The calculation of the electric field by this method is equivalent to the introduction of the Green function for the dipole inside the structure. A detailed description of the calculation procedure is given in the Appendix.

In the weak scattering approximation, the contribution of the scattered radiation to the total energy of the radiation can be neglected, and the sum of the absorption coefficient A and the specular reflection R from the sample is 1

$$R + A = 1,\qquad(1)$$

i.e. the energy of the scattered radiation is much smaller than that of the coherent radiation. Equation (1) is just the energy conservation law when the transmittance equals to zero. The point here is that the transmittance of the considered system is negligible due to the thickness of the metal sublayer.
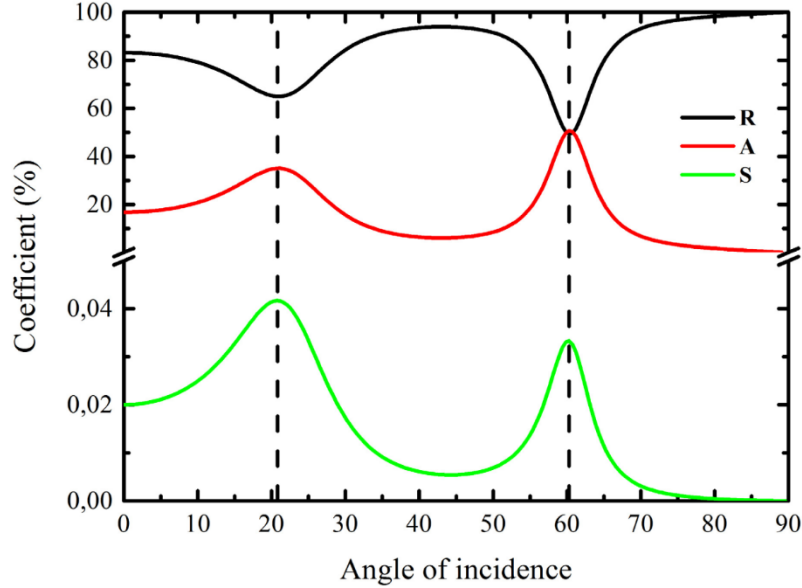

Fig. 2. Dependences of the specular reflection (R), absorption (A) and scattering (S) coefficients on the incidence angle of s-polarized radiation. The thickness of the CeO_2 film is 2100 nm, the refractive index is $n_{CeO2} = 2.2$. The parameters of the Al sublayer: $d_{Al} = 200$ nm, $n_{Al} = 1.26 + 7.28i$ [44]. The refractive index of the substrate is $n_{Al2O3} = 1.70$. The wavelength is 632.8 nm. The vertical dashed lines indicate the angle of mode excitation (see Eq. (6)). The scattering coefficient curve is normalized to a particular value at 0°.

The scattering coefficient S is the ratio between the total intensity of light scattered in the upper hemisphere to the intensity of the incident light. As far as the scattering by different inhomogeneities is considered to be incoherent one, the scattering coefficient is

$$S = \frac{c}{4\pi I_0} N \int_{-d_{CeO_2}}^{0} dz \left| \oint \lim_{r \to \infty} \left(r^2 \sum_{i=s,p} \vec{E}_i^\infty (\hat{r}, r) \times \vec{H}_i^\infty (\hat{r}, r) \right) \hat{\vec{r}} d\Omega \right| \qquad (2)$$

where $\vec{E}_i^\infty$ and $\vec{H}_i^\infty$ are dipole fields at a large distance from the sample, I_0 is the incident light intensity, N is the inhomogeneities concentration and the integration is taken over all the inhomogeneities in the CeO_2 layer. The integral of the Poynting vector

$$\oint \lim_{r \to \infty} \left(r^2 \sum_{i=s,p} \vec{E}_i^\infty (\hat{r}, r) \times \vec{H}_i^\infty (\hat{r}, r) \right) \hat{\vec{r}} d\Omega$$

is taken over the upper hemisphere (the scattering in the lower hemisphere tends to zero due to the nontransparent metal layer). The index i stands for the polarization of scattered radiation. Substituting the Eqs. (17) and (24)–(28) of the Appendix one gets

$$S = \frac{N}{I_0} \int_{-d_{CeO_2}}^{0} dz \left| \oint \left(\vec{S}_p + \vec{S}_s \right) \hat{\vec{r}} d\Omega \right| \qquad (3)$$

where $\vec{S}_s$ and $\vec{S}_p$ are the Poynting vectors of plane waves induced by a single dipole in the direction $\hat{r}$ (see axes in Fig. 1) given by the formulas

$$\vec{S}_s\left(k_x,k_y,z\right) = \frac{c}{8\pi}k_z^2\left|E_{coh}\left(z\right)\right|^2\left|\frac{\alpha k_x k_0^2}{k_\parallel k_z}\right|^2\left|t_+^s\left(k_x,k_y,z\right)\right|^2\hat{k} \tag{4},$$

$$\vec{S}_p\left(k_x,k_y,z\right) = \frac{c}{8\pi}k_z^2\left|E_{coh}\left(z\right)\right|^2\left|\frac{\alpha k_0 k_y}{k_\parallel}\right|^2\left|t_+^p\left(k_x,k_y,z\right)\right|^2\hat{k} \tag{5}$$

where $k_0 = \omega/c$ is the wavenumber in the vacuum, $\left(k_x,k_y,k_z = \sqrt{k_0^2 - k_x^2 - k_y^2}\right)$ is the wavevector (see axes in Fig. 1) of a plane wave propagating in the direction $\hat{r} = \hat{k}$ and $k_\parallel = \sqrt{k_x^2 + k_y^2}$. Here $E_{coh}\left(z\right)$ is the amplitude of coherent field at point z inside the film ($\vec{E}_{coh} \parallel Oy$), α is the polarizability of the inhomogeneity, $t_+^i\left(k_x,k_y,z\right)$ is the effective transmission coefficient (which is given in Appendix and is not equal to Fresnel transmission coefficient) of i polarized scattered wave $\left(k_x,k_y\right)$ to the upper hemisphere. It should be noted, that the dipole radiates a pair of plane waves with the wavevectors $\left(k_x,k_y,\pm k_z\right)$, which both contribute to the transmitted wave amplitude (see Appendix). The Eq. (4) and Eq. (5) are the extension of the perturbation theory for surface scattering [29] to the case of volume scattering.

Figure 2 shows the calculated dependences of the specular reflection, absorption and scattering coefficients of s-polarized radiation at the incidence angle. The calculated values of the reflection and absorption correspond to the system without defects and density fluctuations, and the transformation of the coherent radiation energy to that of the incoherent one is not taken into account (it is assumed that the latter is infinitesimally small). The scattering coefficient curve is normalized for clarity.

To clarify the physical meaning of the scattering and absorption peaks in Fig. 2, the eigenmodes of the considered system should be taken into account. One can distinguish radiation (unbound) and localized (guided) modes of the system.

The localized modes are the guided modes of a planar waveguide. They are localized inside the layer due to the total internal reflection from the boundaries of the layer. The mode propagates through the layer and loses its energy only due to the absorption in the material.

The radiation modes of the waveguide are unbound modes, which are not confined to the waveguide. In contrast to the guided modes, these modes have losses caused by the light transmission through the boundaries of the system (see Fig. 3). The main interest is focused on the resonant radiation modes (RRM) of the waveguide. These modes are specific modes of Fabry-Perot type.
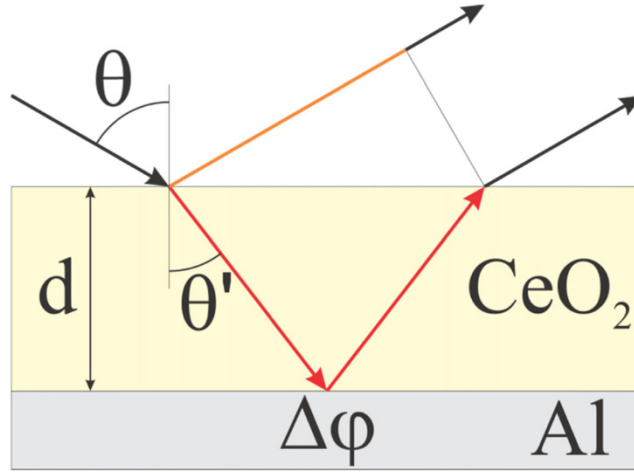
Fig. 3. A dielectric waveguide (CeO$_2$) placed on a metal sublayer(Al).

The RRM excitation condition is the phase matching (see Fig. 3). Taking into account the additional phase shift upon reflection from the Al sublayer, the RRM excitation condition can be written as

$$2dnk_0 \cos\theta' + \Delta\varphi = 2\pi m, \ m \in Z, \tag{6}$$

where

$$\Delta\varphi = \arg\left(r_{CeO_2/Al}\right) = \arg\left(\frac{Y_{CeO_2} - Y_{Al}}{Y_{CeO_2} + Y_{Al}}\right) \tag{7}$$

is a phase jump at the boundary CeO$_2$/Al. Here, $r_{CeO_2/Al}$ is the reflection coefficient of light incident from the half-space of CeO$_2$ onto the aluminum half-space, Y_{CeO_2} and Y_{Al} are the angular admittances for the corresponding materials [45], which are

$$Y = \begin{cases} \sqrt{\varepsilon - k_\parallel^2/k_0^2} \,, s-polarized\ wave \\ \varepsilon/\sqrt{\varepsilon - k_\parallel^2/k_0^2} \,, p-polarized\ wave \end{cases} \tag{8}$$

where $k_\parallel$ is the wavevector component parallel to the layer surface, ε is a medium dielectric permittivity and medium magnetic permeability $\mu = 1$. It is worth mentioning that condition (6) indicates that there is a strong absorption in the system. It is essentially a condition of the Salisbury screen [46].

The excitation of the RRM by the incident wave leads to enhancement of the electric field inside the CeO$_2$ layer (see Fig. 4). The dipole moment representing the inhomogeneity increases as its value is directly proportional to the electric field. Hence, the scattered field increases. At the same time, light absorption increases due to the electromagnetic energy concentration inside the system.
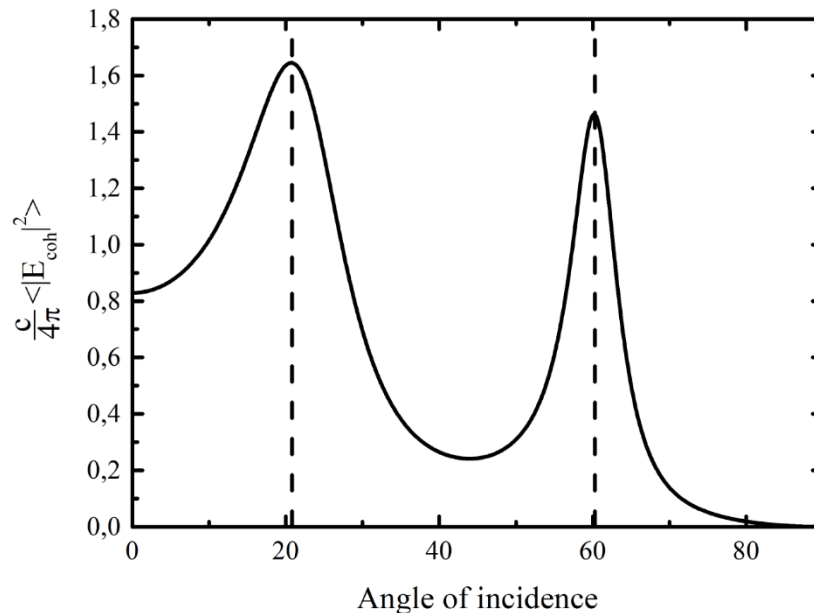
Fig. 4. Dependence of $\left|E_{coh}\right|^2$ averaged across the CeO$_2$ layer on the angle of incidence. The incident wave is s-polarized. The thickness of the CeO$_2$ film is 2100 nm, the refractive index is n_{CeO2} = 2.2. The parameters of the Al sublayer: d_{Al} = 200 nm, n_{Al} = 1.26 + 7.28i [44]. The refractive index of the substrate is n_{Al2O3} = 1.70. The wavelength is 632.8 nm. The Poynting vector of the incident wave is normalized to 1. The dashed lines mark the position of modes (6) excitation.

The considered model reflects the effect of increasing the scattering observed in the real system. When the coherent laser beam illuminates the sample at the angle corresponding to the excitation of an RRM, a considerable part of the beam energy is transferred to the mode of the system. The peaks in Fig. 4 represent the increase of coherent electric field inside the film when the RRMs are excited. The radiation mode propagates inside the film, where its energy is dissipating due to inhomogeneities and absorbed due to Ohmic losses in aluminum. Thus, the coherent radiation is transformed into the dipoles radiation through the RRM, and the scattering increases sharply (see Fig. 2). At the same time, the absorption coefficient also increases.

A similar effect was observed for air/Ag/MgF$_2$/Ag layered system [8]. It was shown that at the angles corresponding to the excitation of the guided modes, light scattering by the surface roughness increases. Thus, the scattering amplification effect is observed when either a guided mode or a resonant radiation mode (Fabry-Perot resonator mode) is excited.

To summarize, it can be concluded that the excitation of the waveguide RRM at a certain angle of incidence leads to the concentration of the incident wave radiation inside the film. The radiation greatly increases both the scattering associated with the presence of inhomogeneities and the absorption due to Ohmic losses in aluminum. Therefore, at certain angles of incidence corresponding to the resonant radiation modes, both scattering and absorption coefficient maxima can be observed.

3.2. Strong scattering

As it was mentioned earlier, the CeO$_2$ film possesses the inhomogeneous structure. The film contains various types of defects (gaps separating the facets of CeO$_2$, surface roughness of the film, surface roughness of the Al sublayer, volume density inhomogeneities) acting as light scattering centers. Coherent radiation scattering by inhomogeneities of different types results

in the transfer of its energy to that of the incoherent radiation. If the scattering is sufficiently strong (a considerable part of the energy is transferred), it is necessary to solve a self-consistent problem; i.e. the coherent radiation energy losses due to the scattering should be taken into account. To formulate the self-consistent problem, we introduce the effective absorption of the coherent radiation in the CeO_2 film as an additional imaginary part of the CeO_2 effective refractive index

$$n_{CeO_2}^{eff} = n_{CeO_2} + in_{sc}. \tag{9}$$

The introduced value n_{sc} should describe the transfer of the coherent radiation into the spatially incoherent component. The introduction of an effective refractive index is, in general, an approximation. However, that approximation is asymptotically exact in many important cases [47,48]. The value of n_{sc} depends on the concentration and scattering cross-section of all the inhomogeneities located inside the film. To clarify the meaning of n_{sc}, one should consider the propagation of a coherent radiation beam through a homogeneous medium containing scatters. The intensity attenuation of the coherent radiation across section dx can be described by solution to the approximated transport equation [14]

$$I(x) = I_0 \exp\left(-\sigma_{eff} N_{eff} x\right) = I_0 \exp\left(-2n_{sc} k_0 x\right) \tag{10}$$

where σ_{eff} and N_{eff} are the effective cross section and concentration of inhomogeneities, k_0 is the wavenumber in vacuum. In this approximation the problem of scattering by different scatterers reduces to a single parameter problem, where the intensity attenuation is described by $n_{sc} = \sigma_{eff} N_{eff} / 2k_0$.

For the numerical simulation the value $n_{sc} = \sigma_{eff} N_{eff} / 2k_0 = 0.01$ was chosen. This value corresponds to analytical evaluation of light scattering in inhomogeneous CeO_2 film.

It should be noted that the imaginary part of the effective refractive index, in this case, is not responsible for the absorption (absorption occurs only in the aluminum layer) and rather describes the transfer of coherent radiation to an incoherent radiation.

The transfer of the energy from the coherent radiation to the incoherent one is calculated as follows

$$I_{tr} = \frac{\omega}{8\pi} \frac{2n_{sc} n_{CeO_2}}{\cos\theta} \int_{-d_{CeO_2}}^{0} \left| E_{coh}(z) \right|^2 dz = \frac{\omega}{8\pi} \frac{\sigma_{eff} N_{eff}}{k_0 \cos\theta} n_{CeO_2} \int_{-d_{CeO_2}}^{0} \left| E_{coh}(z) \right|^2 dz \tag{11}$$

where θ is the angle of incidence and the integration is taken over the CeO_2 layer. The transferred energy is partly absorbed in the aluminum layer and the rest of it is radiated into the upper hemisphere. Thus, the total absorption coefficient A is the sum of the coherent A_{coh} and incoherent A_{incoh} radiation absorption coefficients.

According to the energy conservation law, the sum of the scattering (S) and absorption ($A = A_{coh} + A_{incoh}$) coefficients is

$$S + A_{incoh} + A_{coh} = 1 - R, \tag{12}$$

Both the absorption in aluminum and the scattering in cerium dioxide lead to the losses in coherent radiation energy. The coherent radiation losses in the aluminum are

$$A_{coh} = \frac{\omega}{8\pi} \frac{Im(\varepsilon_{Al})}{I_0 \cos\theta} \int \left| E_{coh}(z) \right|^2 dz \tag{13}$$

where the integration is taken over the aluminum layer. The rest part of the absorption is the absorption of scattered light in the aluminum (A_{incoh}).

The calculated reflectance, absorption and scattering coefficients as functions of the s-polarized laser beam incidence angle are shown in Fig. 5. The reflectance R is calculated by the T-matrix method.
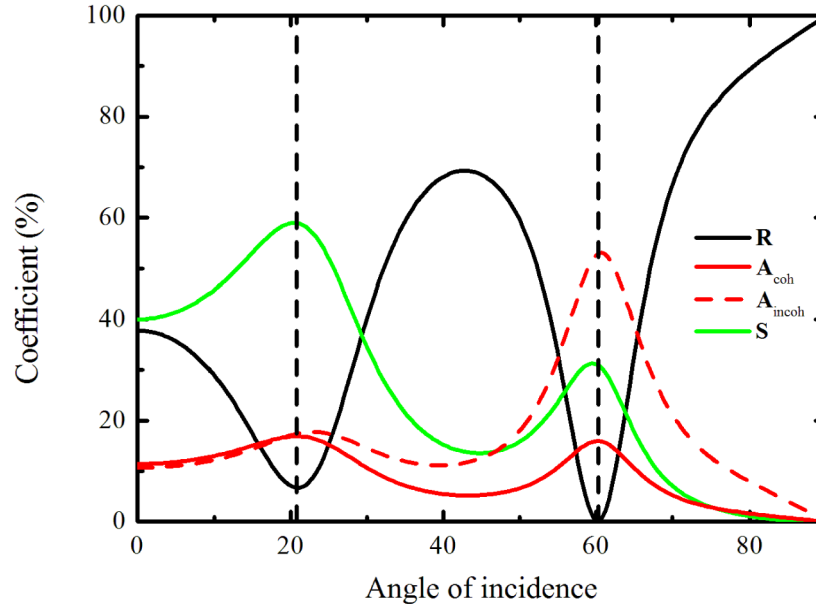

Fig. 5. Dependences of the specular reflection (R), scattering (S), coherent (A_{coh}) and incoherent (A_{incoh}) radiation absorption, coefficients on the incidence angle of s-polarized radiation. The thickness of the CeO_2 film is 2100 nm, the refractive index is $n_{CeO2} = 2.2 + 0.01i$. The parameters of the Al sublayer: $d_{Al} = 200$ nm, $n_{Al} = 1.26 + 7.28i$ [44]. The refractive index of the substrate is $n_{Al2O3} = 1.70$. The wavelength is 632.8 nm. The vertical dashed lines indicate the angle of radiation mode excitation (see Eq. (6)).

The angular dependencies calculated in the framework of the considered simple model are depicted in Fig. 5. The dashed line indicating the Fabry-Perot mode (RRM) excitation angle coincides with the minimum of the reflection curve. That confirms the strong dependence of scattering and absorption coefficients maxima on the Fabry-Perot resonant modes. The reflection coefficient is significantly smaller in comparison to the case of the system without scattering (see Fig. 2). The revealed nature of scattering and absorption coefficients maxima opens up great prospects for manipulating of the reflection from inhomogeneous films.

4. Scattering pattern

Let us consider amplitudes of scattered radiation at a specific angle of incidence. According to our simple model the numerical calculations (see Appendix for details) result in the scattering patterns presented in Fig. 6(a). The appearance of scattering halos on the graphs can be explained by means of Eqs. (4) and (5). The maximum in the scattering pattern occurs if the effective transmission coefficient of the scattered wave $t_+^i\left(k_x, k_y, z\right)$ reaches the maximum, i.e. if the resonant mode (6) is excited. The condition (6) is azimuth-independent leading to the circle-like positions of the scattering maxima on the pattern.
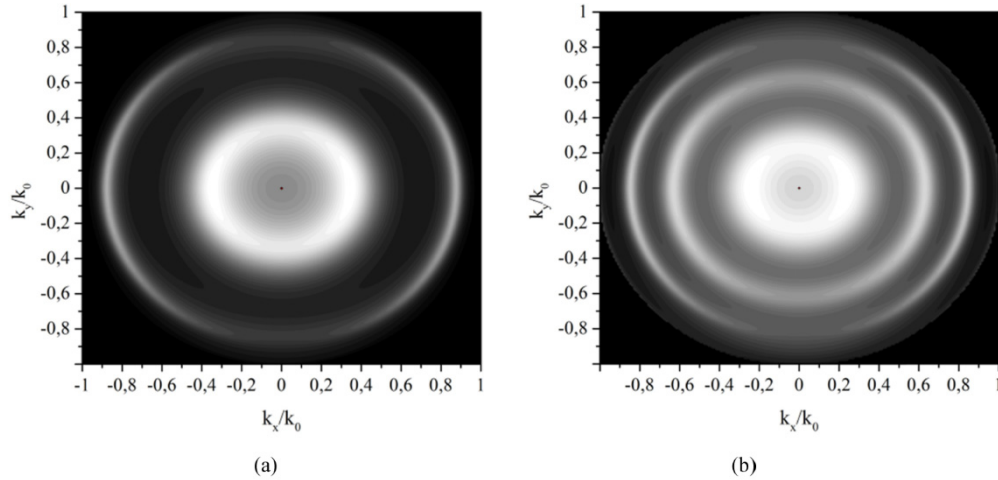
Fig. 6. The intensities of radiation scattered in the air above the systems. The incident light is s-polarized. Each point represent the intensity of radiation scattered to direction $\left(k_x, k_y, k_z = \sqrt{k_0^2 - k_x^2 - k_y^2} \right)$ (see axes in Fig. 1). The figures correspond to cases of (a) the CeO$_2$ waveguide on metal (the parameters of the system are the same as in Fig. 2) (b) the CeO$_2$ waveguide with thickness 4200 nm (n_{CeO2} = 2.2).

The distinct scattering lobes can be seen in Fig. 6(a). The scattering pattern of a CeO$_2$ waveguide is given in Fig. 6(b) for comparison. The thickness of the waveguide is 4200 nm (i.e. it is twice as thick as the system considered before). It can be seen that in Fig. 6(b) there are three halos, which correspond to the Fabry-Perot resonator modes of the waveguide. The scattering pattern of considered coating is similar to that of the waveguide, however without the middle halo.

To explain this, let us first consider a planar waveguide of doubled thickness. The excitation condition for Fabry-Perot resonator modes is the phase matching condition, which can be written in the form

$$4dnk_0 \cos \theta' = 2\pi m_2, \quad m_2 \in Z. \tag{14}$$

At the same time the RRM excitation condition for the dielectric layer placed on a perfect electric conductor takes form

$$2dnk_0 \cos \theta' + \pi = 2\pi m_1, \quad m_1 \in Z. \tag{15}$$

It can be seen from Eq. (14) and (15)

$$m_2 = 2m_1 - 1, \quad m_{1,2} \in Z. \tag{16}$$

In other words the excitation of the odd Fabry-Perot mode of the waveguide occurs at the same angle as the excitation of dielectric layer RRM placed on the perfect electric conductor.

The dielectric permittivity of aluminum in the optical range has a large negative real part (n_{Al} = 1.26 + 7.28i at the wavelength of 632.8 nm [44]). Therefore, the aluminum layer can be considered as a mirror. Thus, the modes in the system under investigation correspond to the odd modes of a waveguide of cerium oxide having double thickness. Numerical consideration of condition (6) confirms this result.Thus, resonant radiation modes manifest themselves both in total scattering in the system and in the scattering patterns of the system for light incident at some arbitrary angle. The radiation scattered by the film inhomogeneities is concentrated in a specific direction. That occurs due to the resonant radiation modes' excitation. As a result,

the halos appear on the scattering patterns of the inhomogeneous film. The condition of halo excitation is quite common for the layered system (compare Fig. 6(a) and Fig. 6(b)).

As it can be seen, each halo in Fig. 6 looks like two separate lobes rather than a single continuous halo. That anisotropy is the result of polarized light scattering: for s-polarized incident wave the induced dipole moments of all inhomogeneties are parallel to the incident light electric field. Thus, the scattered radiation has minimum in the direction due to the anisotropy of a dipole scattering pattern. The calculated scattering patterns are anisotropic as result of the polarized light scattering.

5. Summary

The scattering of the coherent electromagnetic radiation by inhomogeneities of the dielectric metafilm is considered in the paper. The scattering is theoretically studied in terms of the single-scattering approximation. It is shown that the enhancement of the scattering and absorption of the incident-coherent wave occurs at the angles of incidence when the resonant radiation modes (the modes of a Fabry-Perot resonator) are excited. Thus, the increase in scattering and absorption occurs due to the field enhancement inside the film by the resonant radiation modes of the system.

Numerical studies show that scattering can significantly decrease the reflection from the system. For the considered metafilm the reflectance becomes almost zero at the angle of resonant radiation mode excitation. This effect opens an opportunity for manipulating (tuning) the reflectance from inhomogeneous films.

The scatter patterns show the anisotropic properties caused by the system eigenmodes. Namely, the light scattered by the inhomogeneities is concentrated in specific directions due to the excitation of different resonant radiation modes of the waveguide. As a result, series of halos appear on the scatter pattern.

Appendix

We consider a single dipole inside the layer of CeO_2 (see Fig. 7). The magnitude of the dipole will be assumed to be linearly dependent on the magnitude of the field

$$\vec{d} = \alpha \vec{E}(x, y, z) \tag{17}$$

where α is the inhomogeneity polarizability. In other words, in our model the orientation and magnitude of the dipoles are determined by the distribution of the coherent electric field in the sample. The magnitude of the electric field of the coherent radiation is calculated by using the T-matrix method [45].
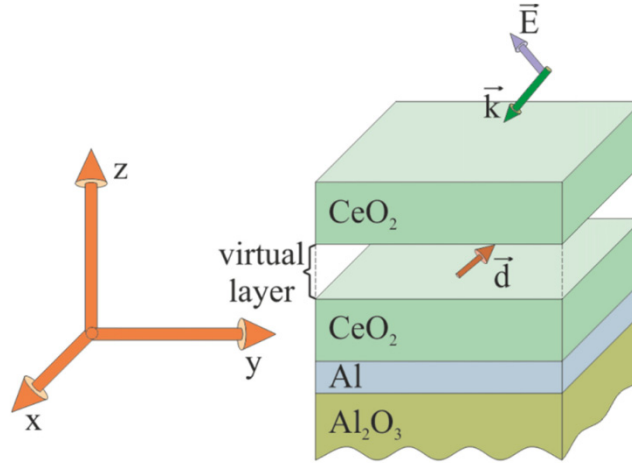
Fig. 7. Model of a system with a dipole scatterer.

In the statement of the scattering problem given in the paper, the calculation of the scattered light amplitudes is equivalent to the calculation of the dipole-induced field. The following approach to the field calculation is equivalent to the calculation of Green function for a dipole placed into the structure under consideration.

The dipole acts as a radiating source. Let us consider the dipole radiation in vacuum. We will consider the coordinate system depicted in Fig. 7. The polarization vectors are

$$\vec{e}_s = \left(\frac{k_y}{k_\parallel} \quad -\frac{k_x}{k_\parallel} \quad 0 \right)^T \tag{18}$$

for s-polarization and

$$\vec{e}_p = \left(\frac{k_x k_z}{k k_\parallel} \quad \frac{k_y k_z}{k k_\parallel} \quad -\frac{k_\parallel}{k} \right)^T \tag{19}$$

for p-polarization. Here k is the wavenumber in vacuum, and $k_\parallel = \sqrt{k_x^2 + k_y^2}$. The electric dipole field can be written in the form [49,50]

$$\vec{E} = ik \left(\vec{A} + \frac{1}{k^2} \vec{\nabla} \left(\vec{\nabla}, \vec{A} \right) \right), \tag{20}$$

where $\vec{A}$ is the vector potential of the dipole, equal to

$$\vec{A} = -\frac{i\omega}{c} \frac{e^{ik|\vec{r} - \vec{r}_0|}}{|\vec{r} - \vec{r}_0|} \vec{d}_0 \tag{21}$$

Here, $\vec{r}_0$ is the radius vector of the dipole position, and $\vec{d}_0$ is the dipole moment magnitude. Applying Weyl identity for a spherical wave [51]

$$\frac{e^{ikr}}{r} = \frac{i}{2\pi} \iint \frac{e^{i(k_x x + k_y y + k_z z)}}{k_z} dk_x dk_y, \tag{22}$$

one obtains the expansion over the basis of the plane waves

$$\vec{E}_d = \frac{i}{2\pi} \iint \frac{1}{k_z} \begin{pmatrix} k^2 - k_x^2 & -k_x k_y & -k_x k_z \\ -k_x k_y & k^2 - k_y^2 & -k_y k_z \\ -k_x k_z & -k_y k_z & k^2 - k_z^2 \end{pmatrix} \begin{pmatrix} d_x \\ d_y \\ d_z \end{pmatrix} e^{i(k_x x + k_y y + k_z z)} dk_x dk_y. \tag{23}$$

The expression (23) for the electric field can be decomposed over the plane waves of different polarizations

$$\vec{E} = \frac{i}{2\pi} \iint \left(E^s\left(k_x, k_y\right) \vec{e}_s + E^p\left(k_x, k_y\right) \vec{e}_p \right) e^{i(k_x x + k_y y + k_z z)} dk_x dk_y, \tag{24}$$

where

$$E^s\left(k_x, k_y\right) = \frac{k^2}{k_\| k_z}\left(k_y d_x - k_x d_y\right) \tag{25}$$

for s-polarization and

$$E^p\left(k_x, k_y\right) = \frac{k}{k_\|}\left(k_x d_x + k_y d_y\right) - \frac{k k_\|}{k_z} d_z \tag{26}$$

for p-polarization

It is convenient to calculate the dipole-induced field inside the structure by using the T-matrix method.
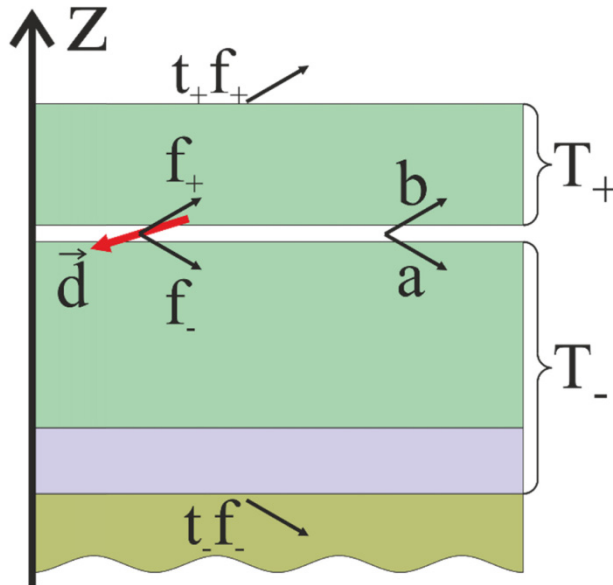

Fig. 8. A dipole placed between two layered subsystems.

It is easier to carry out the calculation by distinguishing two parts of the system: subsystems above and below the dipole (see Fig. 8). Then the dipole is placed inside an infinitely thin layer separating the subsystems. In this case, the radiation of the dipole inside this infinitely thin layer can be described by Eqs. (24)–(26).

The problem of electromagnetic wave propagation can be calculated with the help of T-matrices T_+ and T_-, respectively (see Fig. 8). The field at the upper (lower) boundary of the system can be found by solving the following system of equations

$$\begin{pmatrix} t_+ f_+ \\ 0 \end{pmatrix} = T_+ \begin{pmatrix} f_+ + b \\ a \end{pmatrix}$$

$$\begin{pmatrix} b \\ a + f_- \end{pmatrix} = T_- \begin{pmatrix} 0 \\ t_- f_- \end{pmatrix} \tag{27}$$

where the amplitudes $t_+ f_+$, $t_- f_-$, a, b, f_+, f_- of the waves are shown in Fig. 8. The amplitudes a and b correspond to the waves reflected from the lower and upper subsystems, and f_+ and f_- - are the amplitudes of the waves induced by the dipole (see Eqs. (24)–(26)). The Eq. (27) accounts for the waves f_+ and f_- interference.

Knowledge of the wave amplitude $E_+^{s,p}(k_x, k_y)$ on the upper plane of the system allows one easily obtain the field at infinite distance according to the equation

$$E_\infty^{s,p}\left(\frac{x}{r}, \frac{y}{r}, \frac{z}{r}\right) = -ik_z E_+^{s,p}(k_x, k_y)\frac{e^{ikr}}{r}, \quad r \to \infty, \tag{28}$$

where $E_\infty^{s,p}\left(\frac{x}{r}, \frac{y}{r}, \frac{z}{r}\right)$ is the amplitude of polarized light at a large distance in the direction of the vector $\left(\frac{x}{r}, \frac{y}{r}, \frac{z}{r}\right)$. Thus, the scattering amplitude can be calculated. The integrating of the scattering amplitude modulus square over the hemisphere is the hemispherical scattering.

Funding

Acknowledgments

References

1. J. W. Hovenier, C. V. Van der Mee, and H. Domke, *Transfer of polarized light in planetary atmospheres: basic concepts and practical methods*, vol. 318 (Springer Science & Business Media, 2014).
2. S. Chandrasekhar, *Radiative transfer* (Courier Corporation, 2013).
3. E. Moulin, J. Sukmanowski, P. Luo, R. Carius, F. Royer, and H. Stiebig, "Improved light absorption in thin-film silicon solar cells by integration of silver nanoparticles," J. Non-crystalline Solids **354**(19-25), 2488–2491 (2008).
4. C. Bordier, C. Andraud, E. Charron, and J. Lafait, "Radiative transfer model with polarization effects applied to organic matter," Physica B **394**(2), 301–305 (2007).
5. R. Garcia and C. Siewert, "A generalized spherical harmonics solution for radiative transfer models that include polarization effects," J. Quant. Spectrosc. Radiat. Transf. **36**(5), 401–423 (1986).
6. R. Garcia, "Radiative transfer with polarization in a multi-layer medium subject to Fresnel boundary and interface conditions," J. Quant. Spectrosc. Radiat. Transf. **115**, 28–45 (2013).
7. B. Aduev, D. Nurmukhametov, G. Belokurov, A. Zvekov, A. Kalenskii, A. Nikitin, and I. Y. Liskov, "Integrating sphere study of the optical properties of aluminum nanoparticles in tetranitropentaerytrite," Tech. Phys. **59**(9), 1387–1392 (2014).
8. A. S. Ramírez-Duverger and R. García-Llamas, "Light scattering from a multimode waveguide of planarmetallic walls," Opt. Commun. **227**(4-6), 227–235 (2003).
9. V. Celli, A. A. Maradudin, A. Marvin, and A. R. McGurn, "Some aspects of light scattering from a randomly rough metal surface," J. Opt. Soc. Am. A **2**(12), 2225–2239 (1985).
10. M. Nieto-Vesperinas and J. M. Soto-Crespo, "Monte Carlo simulations for scattering of electromagnetic waves from perfectly conductive random rough surfaces," Opt. Lett. **12**(12), 979–981 (1987).

11. J. A. Sánchez-Gil, A. A. Maradudin, J. Q. Lu, V. D. Freilikher, M. Pustilnik, and I. Yurkevich, "Scattering of electromagnetic waves from a bounded medium with a random surface," Phys. Rev. B Condens. Matter **50**(20), 15353–15368 (1994).

12. R. Garcia and C. Siewert, "A simplified implementation of the discrete-ordinates method for a class of problems in radiative transfer with polarization," J. Quant. Spectrosc. Radiat. Transf. **112**(18), 2801–2813 (2011).

13. A. A. Zvekov, A. V. e. Kalenskii, A. P. Nikitin, and B. P. Aduev, "Radiance distribution simulation in a transparent medium with fresnel boundaries containing aluminum nanoparticles," Comput. Opt. **38**(4), 749–756 (2014).

14. A. Ishimaru, *Wave propagation and scattering in random media* (Academic, 1978).

15. X. Ben, H.-L. Yi, and H.-P. Tan, "Polarized radiative transfer in an arbitrary multilayer semitransparent medium," Appl. Opt. **53**(7), 1427–1441 (2014).

16. C. K. Hayakawa, J. Spanier, and V. Venugopalan, "Comparative analysis of discrete and continuous absorption weighting estimators used in Monte Carlo simulations of radiative transport in turbid media," J. Opt. Soc. Am. A **31**(2), 301–311 (2014).

17. P. Sheng, *Introduction to wave scattering, localization and mesoscopic phenomena*, vol. 88 (Springer Science & Business Media, 2006).

18. R. Garcia, C. Siewert, and A. Yacout, "On the use of fresnel boundary and interface conditions in radiative-transfer calculations for multilayered media," J. Quant. Spectrosc. Radiat. Transf. **109**(5), 752–769 (2008).

19. J. Caron, C. Andraud, and J. Lafait, "Radiative transfer calculations in multilayer systems with smooth or rough interfaces," J. Mod. Opt. **51**(4), 575–595 (2004).

20. R. Elaloufi, S. Arridge, R. Pierrat, and R. Carminati, "Light propagation in multilayered scattering media beyond the diffusive regime," Appl. Opt. **46**(13), 2528–2539 (2007).

21. Z. L. Wang, H. Ogura, and N. Takahashi, "Enhanced scattering from a planar waveguide structure with a slightly rough boundary," Phys. Rev. B Condens. Matter **52**(8), 6027–6041 (1995).

22. T. Kawanishi, H. Ogura, and Z. Wang, "Scattering of an electromagnetic wave from a slightly random dielectric surface: Yoneda peak and Brewster angle in incoherent scattering," Waves Random Media **7**(3), 351–384 (1997).

23. J. Sánchez-Gil and M. Nieto-Vesperinas, "Light scattering from random rough dielectric surfaces," J. Opt. Soc. Am. A **8**(8), 1270–1286 (1991).

24. J. Soto-Crespo, M. Nieto-Vesperinas, and A. Friberg, "Scattering from slightly rough random surfaces: a detailed study on the validity of the small perturbation method," J. Opt. Soc. Am. A **7**(7), 1185–1201 (1990).

25. N. Déchamps, N. de Beaucoudrey, C. Bourlier, and S. Toutain, "Fast numerical method for electromagnetic scattering by rough layered interfaces: Propagation-inside-layer expansion method," J. Opt. Soc. Am. A **23**(2), 359–369 (2006).

26. A. A. Maradudin, E. R. Méndez, and T. Michel, "Backscattering effects in the elastic scattering of p-polarized light from a large-amplitude random metallic grating," Opt. Lett. **14**(3), 151–153 (1989).

27. I. Simonsen and A. A. Maradudin, "Numerical simulation of electromagnetic wave scattering from planar dielectric films deposited on rough perfectly conducting substrates," Opt. Commun. **162**(1-3), 99–111 (1999).

28. Ø. S. Hetland, A. A. Maradudin, T. Nordam, and I. Simonsen, "Numerical studies of the scattering of light from a two-dimensional randomly rough interface between two dielectric media," Phys. Rev. A (Coll. Park) **93**(5), 053819 (2016).

29. E. E. Gorodnichev, S. L. Dudarev, D. Rogozkin, and M. I. Ryazanov, "Coherent effects in backscattering of waves from a medium with random inhomogeneities," Sov. Phys. JETP **66**, 938 (1987).

30. S. K. Sinha, E. B. Sirota, S. Garoff, and H. B. Stanley, "X-ray and neutron scattering from rough surfaces," Phys. Rev. B Condens. Matter **38**(4), 2297–2311 (1988).

31. E. E. Gorodnichev, S. L. Dudarev, D. B. Rogozkin, and M. I. Ryazanov, "Nature of anomalous x-ray reflection from a surface," Sov.Phys. JETP Lett. **48**, 147 (1988).

32. Ø. S. Hetland, A. A. Maradudin, T. Nordam, P. A. Letnes, and I. Simonsen, "Numerical studies of the transmission of light through a two-dimensional randomly rough interface," Phys. Rev. A (Coll. Park) **95**(4), 043808 (2017).

33. F. Brouers, S. Blacher, and A. K. Sarychev, "Giant field fluctuations and anomalous light scattering from semicontinuous metal films," Phys. Rev. B Condens. Matter Mater. Phys. **58**(23), 15897–15903 (1998).

34. M. Breit, V. Podolskiy, S. Grésillon, G. Von Plessen, J. Feldmann, J. Rivoal, P. Gadenne, A. K. Sarychev, and V. M. Shalaev, "Experimental observation of percolation-enhanced nonlinear light scattering from semicontinuous metalfilms," Phys. Rev. B Condens. Matter Mater. Phys. **64**(12), 125106 (2001).

35. E. Chaikina, P. Negrete-Regagnon, V. Ruiz-Cortés, and E. Méndez, "Measurements of the hemispherical scattering distribution function of rough dielectric surfaces," Opt. Commun. **208**(4-6), 215–221 (2002).

36. I. Kurochkin, I. Ryzhikov, A. Sarychev, K. Afanasiev, I. Budashov, M. Sedova, I. Boginskaya, S. Amitonov, and A. Lagarkov, "New sers-active junction based on cerium dioxide facet dielectric films for biosensing," Adv. Electromagn. **3**(1), 57–60 (2014).

37. E. Khawaja, S. Durrani, and M. Al-Kuhaili, "Determination of average refractive index of thin CeO_2 films with large inhomogeneities," J. Phys. D Appl. Phys. **36**(5), 545–551 (2003).

38. I. Hodgkinson, S. Cloughley, Q. H. Wu, and S. Kassam, "Anisotropic scatter patterns and anomalous birefringence of obliquely deposited cerium oxide films," Appl. Opt. **35**(28), 5563–5568 (1996).

39. R. Bueno, J. Martinez-Duart, M. Hernandez-Velez, and L. Vazquez, "Optical and structural characterization of rf sputtered CeO_2 thin films," J. Mater. Sci. **32**(7), 1861–1865 (1997).
40. M. Anwar, S. Kumar, F. Ahmed, N. Arshi, Y. J. Seo, C. G. Lee, and B. H. Koo, "Study of nanocrystalline ceria thin films deposited by e-beam technique," Curr. Appl. Phys. **11**(1), S301–S304 (2011).
41. S. Kanakaraju, S. Mohan, and A. Sood, "Optical and structural properties of reactive ion beam sputter deposited CeO_2 films," Thin Solid Films **305**(1-2), 191–195 (1997).
42. C. Tian, Y. Du, and S.-W. Chan, "Preparation and microstructural study of CeO_2 thin films," J. Vac. Sci. & Technol. A: Vacuum, Surfaces, Films **15**(1), 85–92 (1997).
43. A. Cavallaro, F. Sandiumenge, J. Gazquez, T. Puig, X. Obradors, J. Arbiol, and H. C. Freyhardt, "Growth mechanism, microstructure, and surface modification of nanostructured CeO_2 films by chemical solution deposition," Adv. Funct. Mater. **16**(10), 1363–1372 (2006).
44. A. D. Rakić, A. B. Djurišić, J. M. Elazar, and M. L. Majewski, "Optical properties of metallic films for vertical-cavity optoelectronic devices," Appl. Opt. **37**(22), 5271–5283 (1998).
45. P. Yeh, *Optical waves in layered media*, vol. 61 (Wiley-Interscience, 2005).
46. W. W. Salisbury, "Absorbent body for electromagnetic waves," US Patent 2,599,944, (1952).
47. R. Puzko and A. Merzlikin, "To the analyticity of the effective refractive index," J. Commun. Technol. Electron. **61**(12), 1368–1373 (2016).
48. R. Puzko and A. Merzlikin, "Analytical properties of the effective refractive index," Opt. Commun. **383**, 323–329 (2017).
49. C.-T. Tai, *Dyadic Green functions in electromagnetic theory* (IEEE, 1994).
50. M. Born and E. Wolf, *Principles of optics: electromagnetic theory of propagation, interference and diffraction of light* (Elsevier, 2013).
51. H. Thorkild and A. D. Yaghjian, *Plane-wave theory of time-domain fields: near-field scanning applications* (IEEE, 1999).